

# Spatial and temporal variations of air temperature inversions over different surface types on Ammassalik Island (East Greenland)

Iris Hansche<sup>1</sup>, Jakob Abermann<sup>1</sup>, Sonika Shahi<sup>1</sup>, Wolfgang Schöner<sup>1,2</sup>

<sup>1</sup>Department of Geography and Regional Science, University of Graz, Austria; <sup>2</sup>Austrian Polar Research Center, Austria

EGU General Assembly 2020

AS2.9 – Polar meteorology and climatology and their link to changes in the cryosphere



# Background



Air temperature inversion, a situation in which atmospheric temperature increases with height, is a common feature in the Arctic planetary boundary layer. This stable layer has multiple consequences for the Arctic environment. While vertical gradients of flora and fauna are impacted by them, they also have a direct consequence on physical characteristics such as permafrost thaw depths and snow cover. Therefore, a comprehensive knowledge about the spatial and temporal variability of temperature inversion characteristics such as thickness, intensity, magnitude and frequency is crucial for the surface impact of Arctic climate change.

Here, we investigate the spatial and temporal variations of temperature inversions over different surface types on Ammassalik Island in East Greenland. During a field campaign in summer 2019, high temporal resolution profiles of atmospheric variables such as air temperature, humidity and pressure were collected using UAVs. We acquired 147 profiles in a period of 13 days (06/07/2019-18/07-2019) over different surface types (rock, gravel, snow, ice) and with varying distance to the ocean (approx. 0-6 km). We found a distinct air temperature inversion present in all the profiles whereby height and thickness differ considerably. Both ocean and ice surface act as near-surface cooling agents, which favours the development of inversions. The ice-free area between ocean and glacier tends to warm up strongly during Arctic summer and those different drivers manifest in an intricate pattern of air temperature stratification along a valley axis.

Our high-frequency and high-resolution profiles are also compared with atmospheric temperature profiles from the nearby Tasiilaq radiosonde to assess the performance and limitations to resolve the atmospheric stratification.



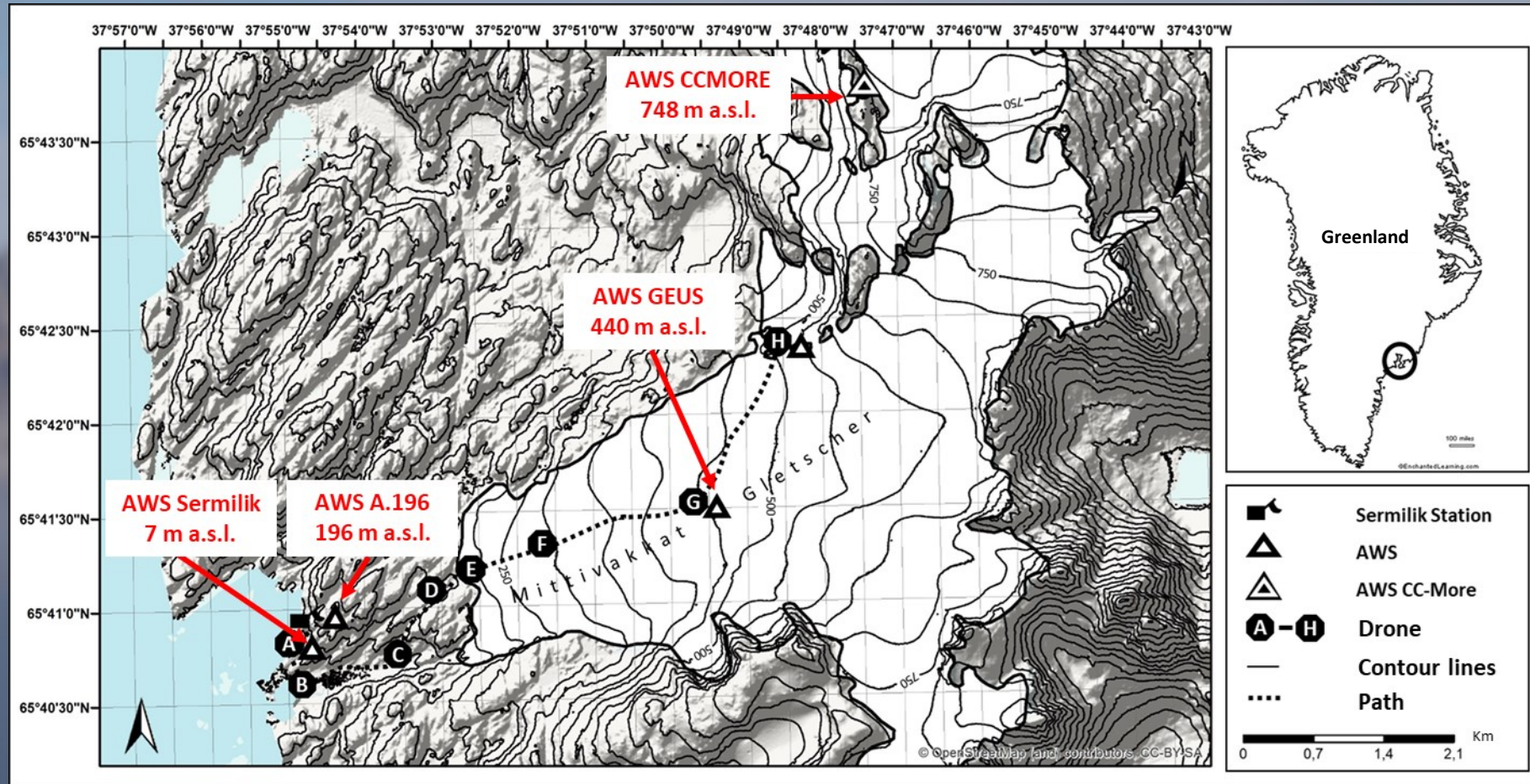
# Data collection



- Field campaign: 06.07.2019 – 18.07.2019
- 3 Drones
  - Mavic Pro
- 3 Sensors
  - iMet-XQ2
    - Temperature
    - Humidity (Sensor broke on the 13<sup>th</sup> of July)
    - Altitude
    - Pressure
    - Coordinates
- Profile above different surfaces
  - Until 500 m a.g.l.
- Simultaneous ascends



# Data collection



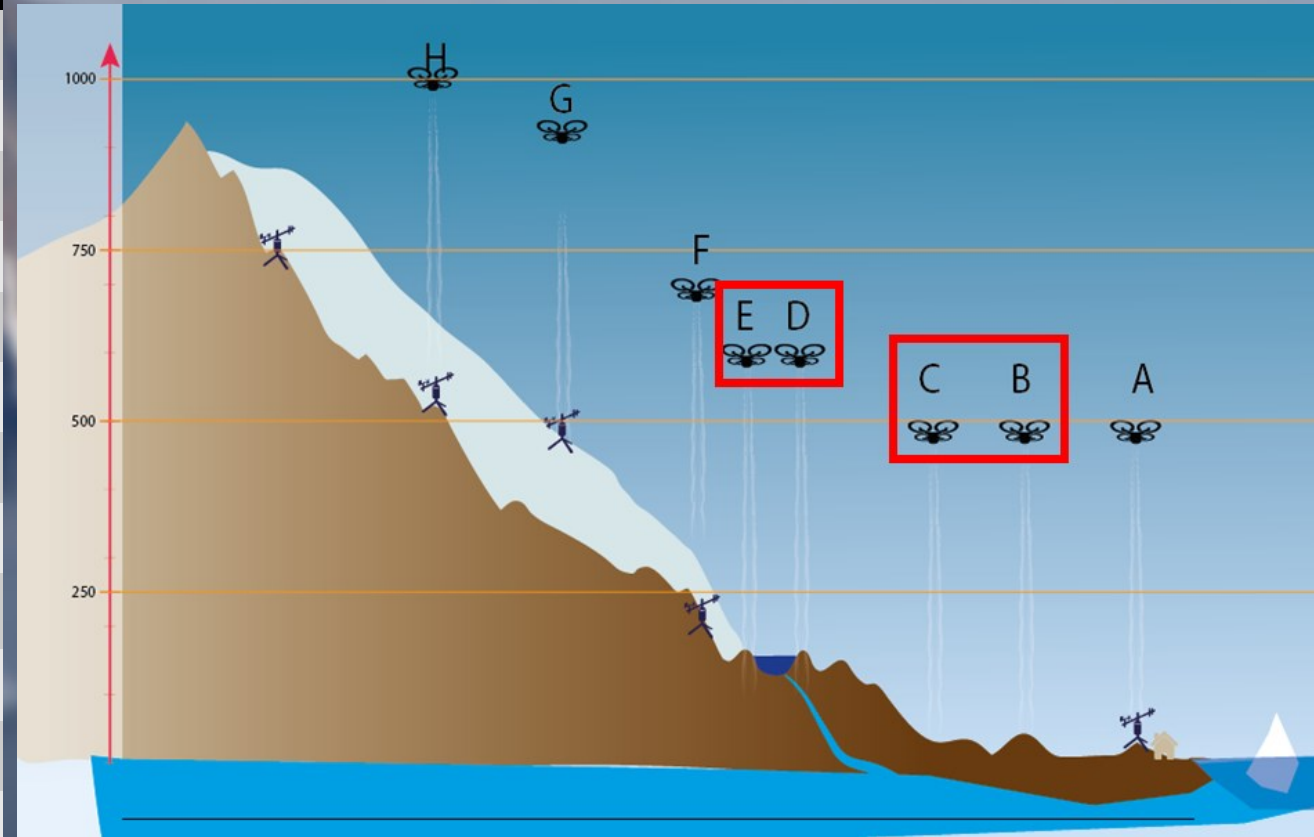
The research area is located on Ammassalik Island in East Greenland around the research station Sermilik (hut symbol). Points A to H indicate the observation points where we took the profiles along our walking path (dashed line). Position A, B, C, D and H are above rock or sand, while position E, F and G are above snow and ice. The triangles show the location of the used AWS transect in the research area. We set up an additional weather station at around 748 m a.s.l. (picture to the right).

# Data collection



Date	Profiles morning - afternoon	Profiles afternoon - evening
07.07.2019		A
08.07.2019	A, B, C, D, E, F, G	F, E, C, B, A
09.07.2019	A, B, C, D, E, F, G, H	F, E, D, C, B, A
10.07.2019	A, B, C, D, E, F, G	E, D, C, B, A
11.07.2019	A, B, C, D, E, F, G, H	F, E, D, C, B, A
12.07.2019	A, A, B, C, D, A, E, A, A, F, A	D, C, A
13.07.2019	A, B, C, D, E, F, G	E, D, C, B, A
14.07.2019	A	A
15.07.2019	A, B, C, D, E, F, G, H	C, B
16.07.2019	A, B, C, D, E, F,	E, D, A
17.07.2019	A, B, D	D, A
18.07.2019	A, C, E, G	F, E, D, B, A

Collected profiles per day during the observation period.



Simultaneous ascents: B, C (approx. 10 m a.s.l.) and D, E. (approx. 150 m a.s.l.)

# Data collection



## Additional data

Radiosonde data have been widely used to study temperature inversions in the Arctic (KAHL 1990; MERNILD 2009; GILSON et al. 2018; YU et al. 2019). Because of the limited vertical resolution of the radiosonde data many of the shallow temperature inversions can not be captured (MERNILD 2009).

In this study, twice daily soundings at 0000 and 1200 UTC from the nearby station Tasiilaq were compared with simultaneously collected drone profiles at the research station Sermilik. In order to detect how well the radiosonde data resolve the atmospheric stratification.



Source: [https://www.dmi.dk/fileadmin/user\\_upload/Rapporter/TR/2015/DMI-TR-15-12.pdf](https://www.dmi.dk/fileadmin/user_upload/Rapporter/TR/2015/DMI-TR-15-12.pdf)



Source: <https://opentopomap.org>

# Definitions

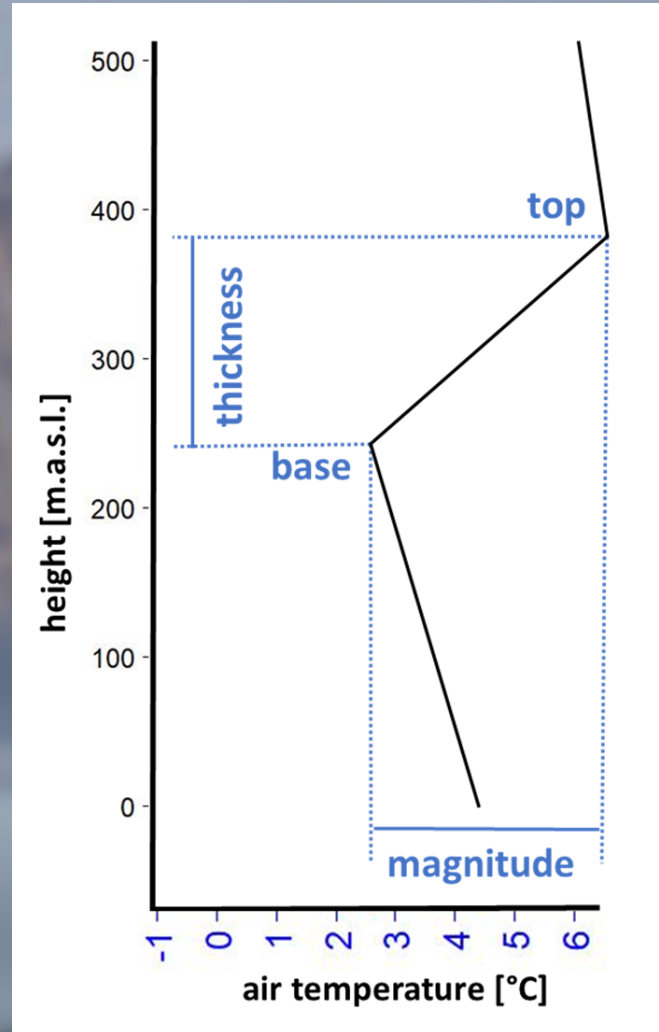


## Inversion (modified after KAHL (1990))

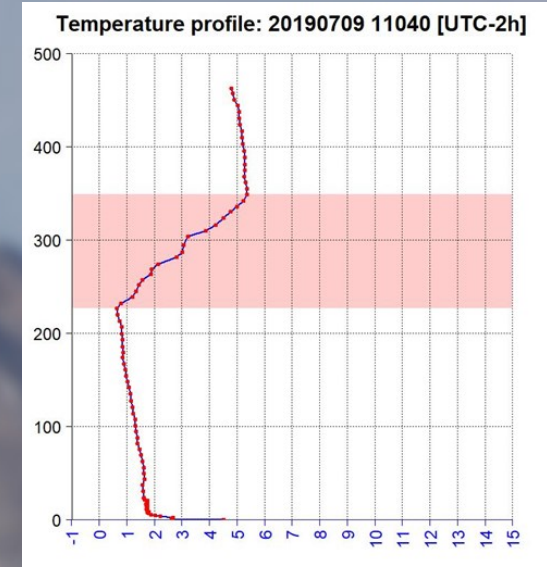
- Atmospheric temperature increases with height ( $\geq 0.1^\circ\text{C}$ ).
- Thin negative-lapse layers  $\leq 50$  m are ignored
- Minimum Inversion thickness
  - $\geq 2$  m (first 20 m a.g.l.)
  - $\geq 5$  m (20 – 500 m a.g.l.)

## • Inversion characteristics

- Inversion base
- Inversion top
- Inversion magnitude
- Inversion thickness
- Inversion frequency
- Inversion type (SBI, EI)



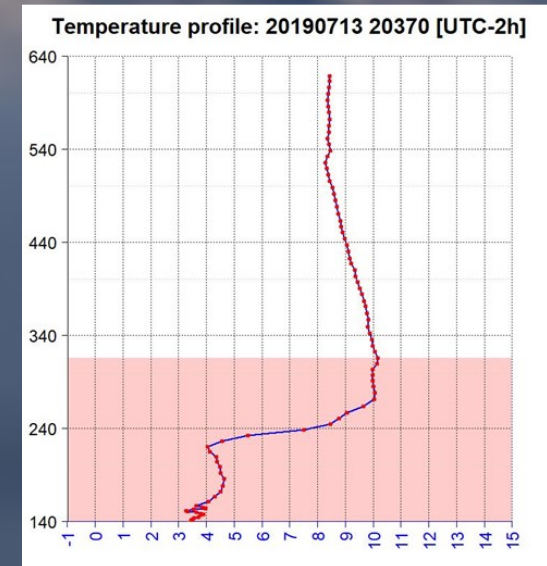
Definition of inversion characteristics



Example of an elevated Inversion (EI).

X-axes: height m a.s.l.

Y-axes: Temperature [°C]



Example of a surface-based Inversion (SBI)

# Inversion detection algorithm

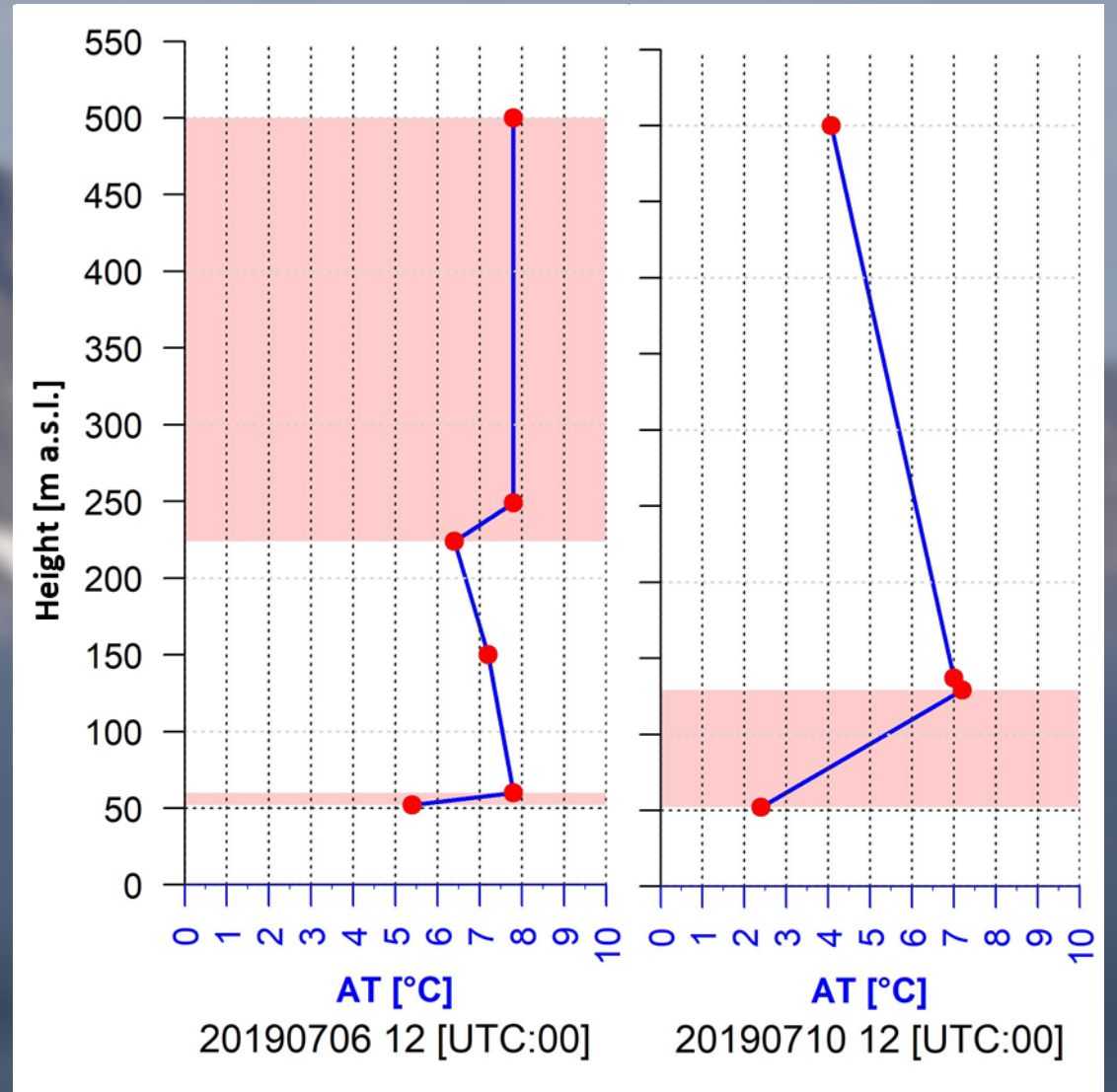
## Task:

- Identifies:
  - All inversion characteristics (base, top...)
  - Inversion 0 1
  - Inversion type

## Output:

- New dataset with all inversion characteristics
- Graphic: visualization of the characteristics
- Statistical output

Examples of inversion detection algorithm visual output (right side) from the radiosonde data. The light red area in the graph indicates the detected inversion layer.



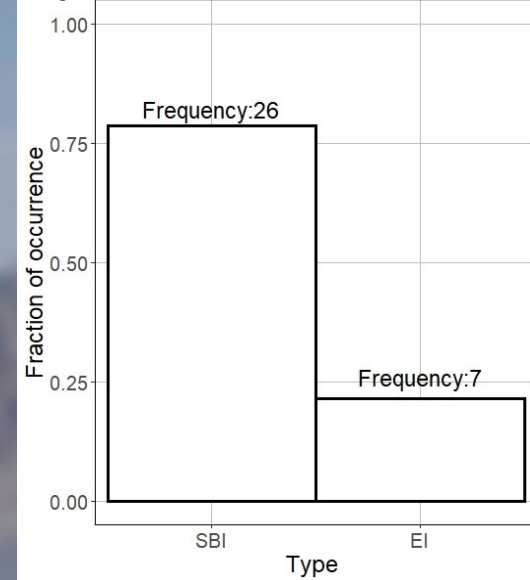
# Radiosonde vs. Drone



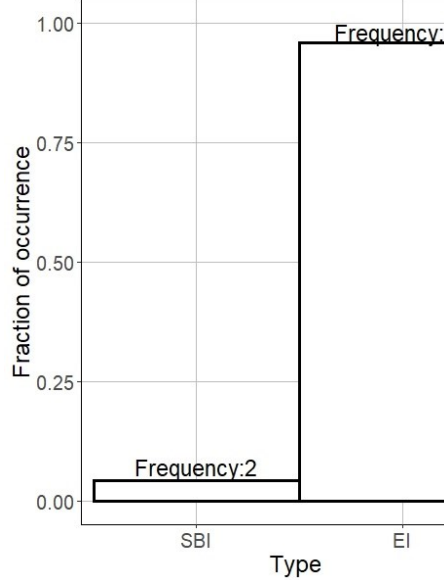
Temperature inversions were detected in all 22 drone observations collected at the same time as the radiosonde observation is taking place (0000 and 1200 UTC) and in 21 of the radiosonde observations. There are more EI in the drone data compared to the radiosonde data. It is exactly the opposite when we look at the SBIs, which are less frequent in the drone data (fig. 1.a).

One reason for the high SBI frequency found in the radiosonde observation could be the low starting temperatures of the radiosonde (examples in figure 1.b green rectangle). Therefore, SBIs were detected in 21 of 22 radiosonde observations. We compared the first point of measurement of the radiosonde (2 m a.g.l., green rectangle in figure 1.b) with the temperature data from the AWS Tasiilaq which is just a few meters away (same time 1200 UTC) (fig. 1.c). We observed a systematic deviation between both measurements. Apart from the 17th July, all radiosonde observations were lower than the AWS by 2-5 °C. There is more similarity between the AWS in Sermilik and the AWS in Tasiilaq than between the radiosonde and the AWS Tasiilaq (fig. 1.d).

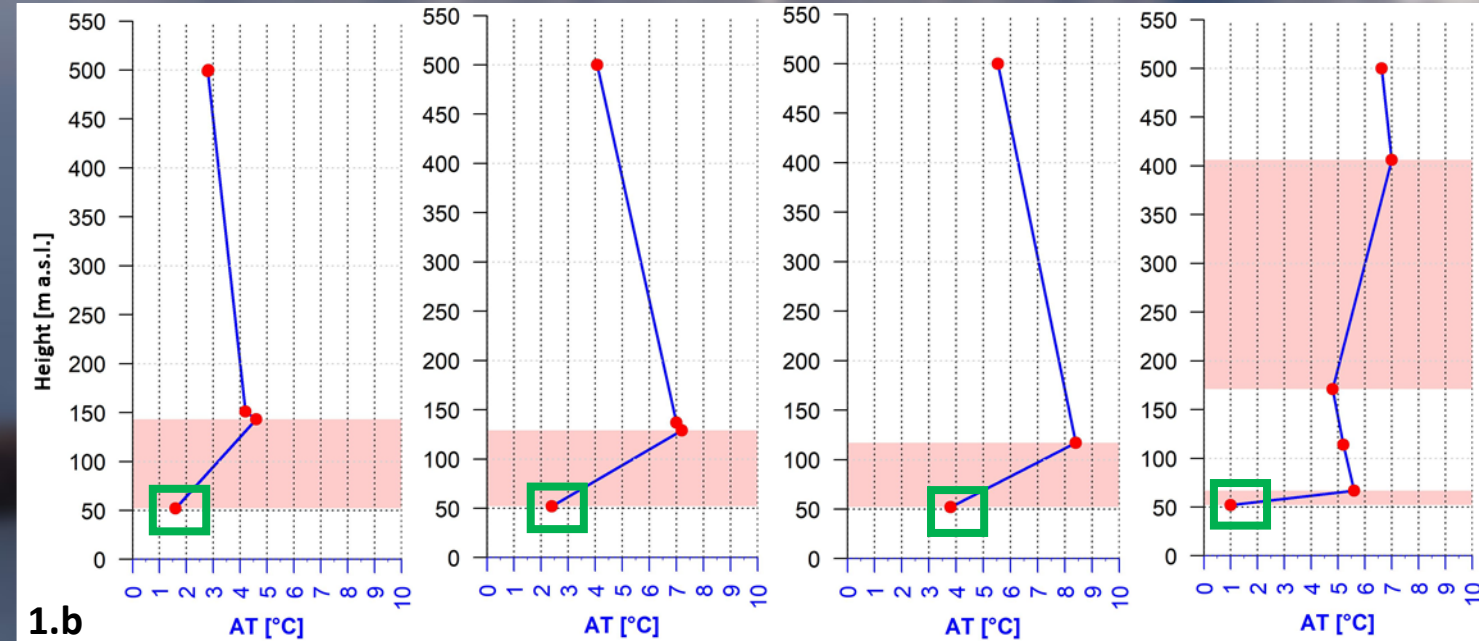
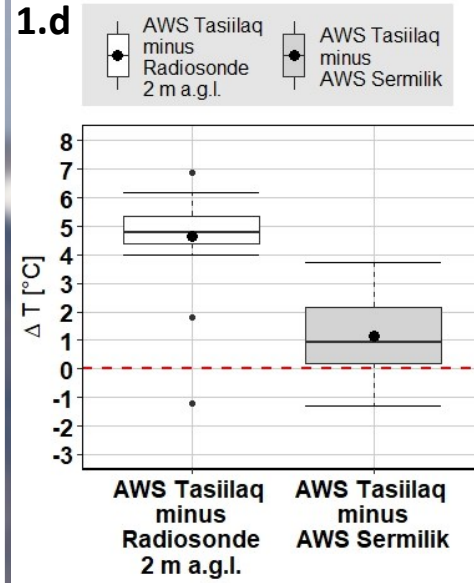
**1.a** Inversion Type frequency Radiosonde



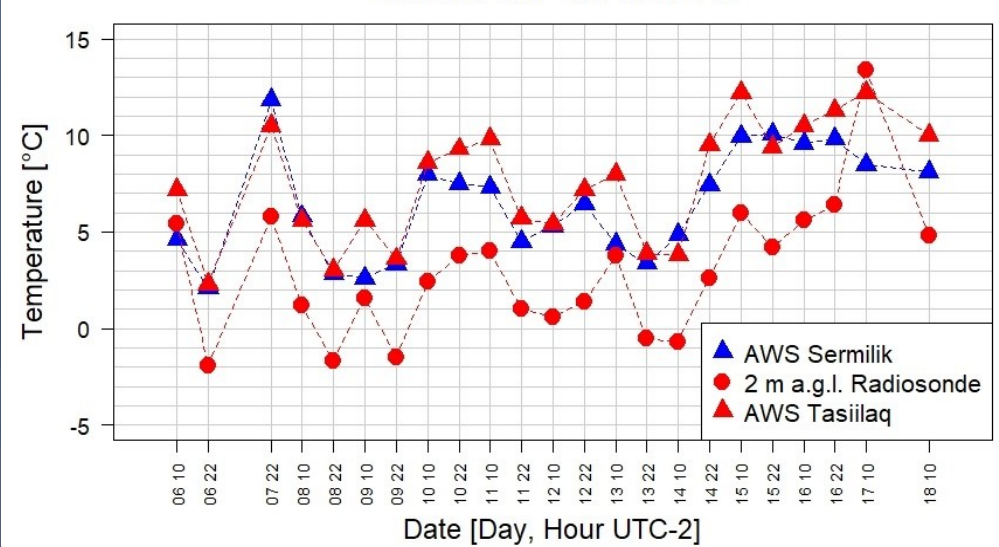
**1.a** Inversion Type frequency Drone



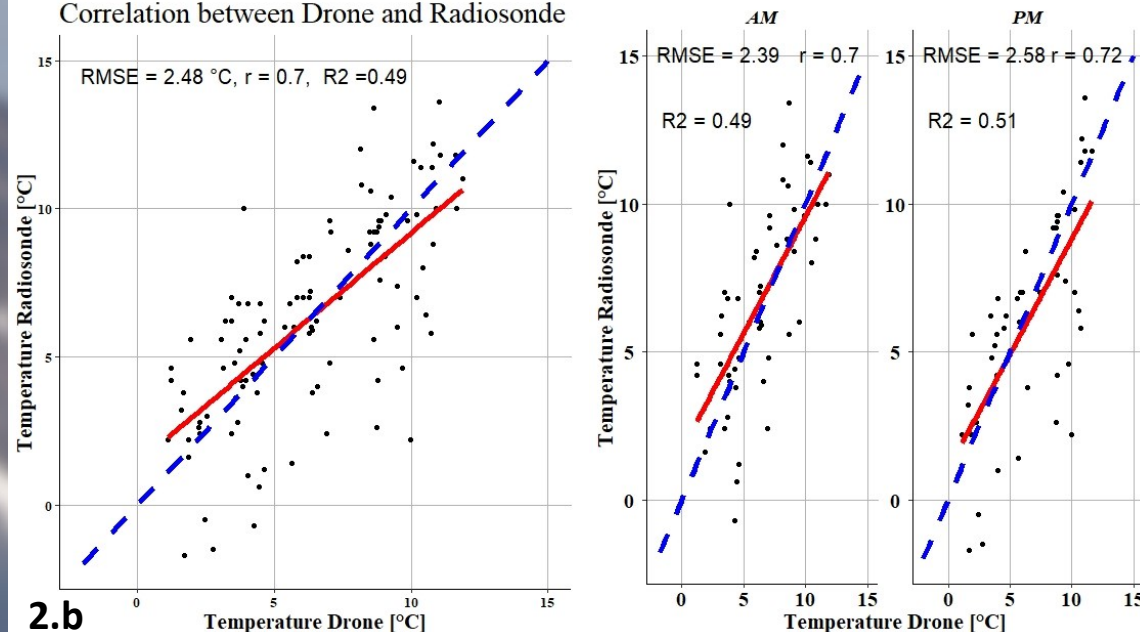
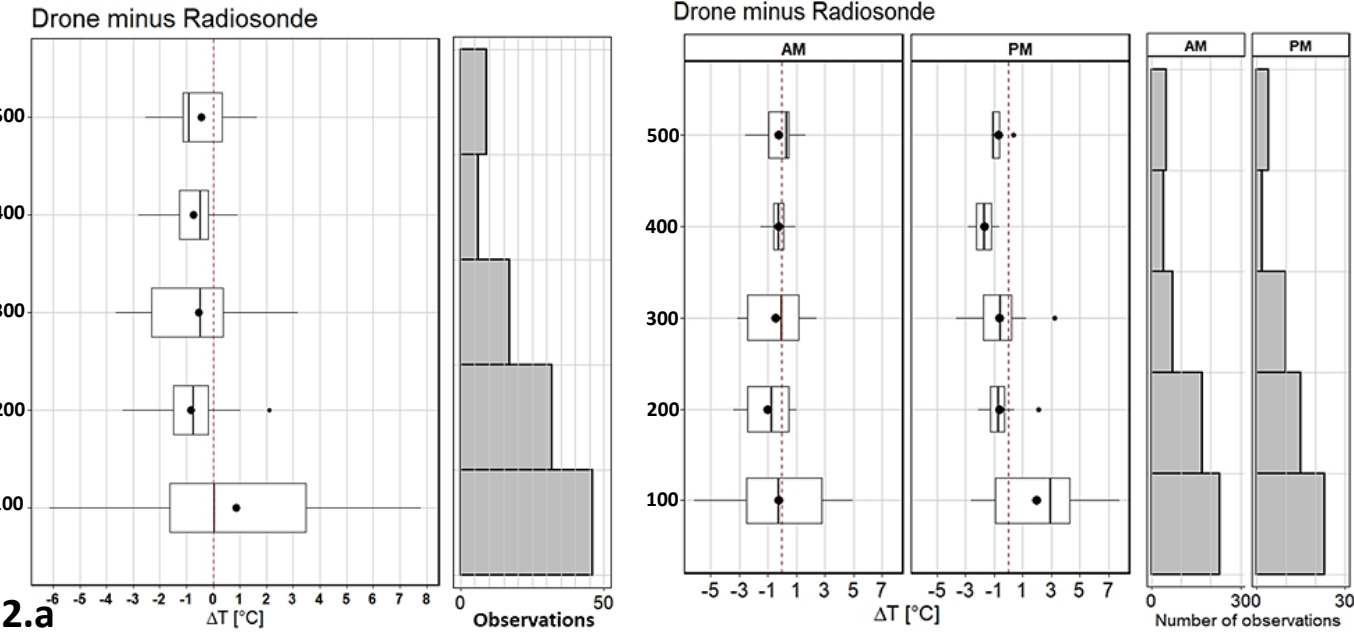
**1.d**



**1.c** Air temperatur Radiosonde, AWS Tasiilaq and Sermilik 2019.07.06 - 2019.07.18



# Radiosonde vs. Drone



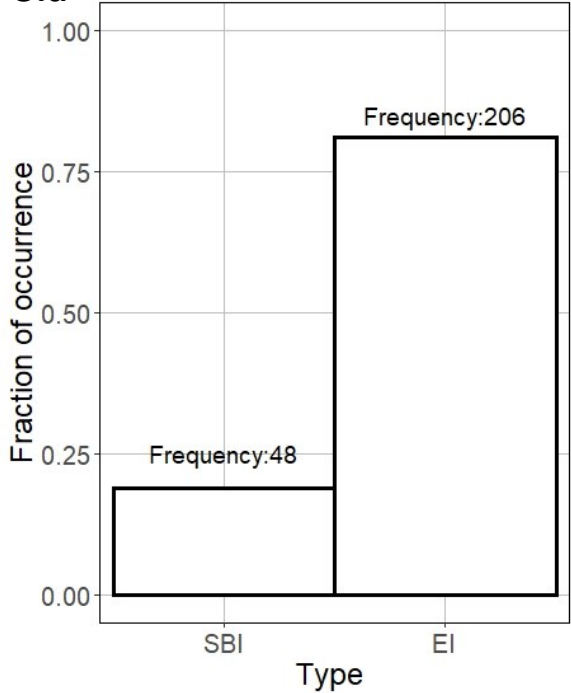
The radiosonde and drone observations were grouped in five elevation bands (**fig. 2.a** y-axes: Height m a.s.l.). Common data points were subtracted from each other (drone minus radiosonde) to detect the elevation with the highest and the lowest deviation. As expected, the first 100 m show the highest deviation (different settings). At higher altitudes, the deviation is getting smaller.

Both data show a relatively strong linear relationship (**fig. 2.b** around  $r=0.7$ ). The root-mean-square-error (RMSE) is approximately 2.5 °C. This error is slightly higher in the PM data, which goes along with a higher deviation of the PM radiosonde data from the drone data (boxplot).

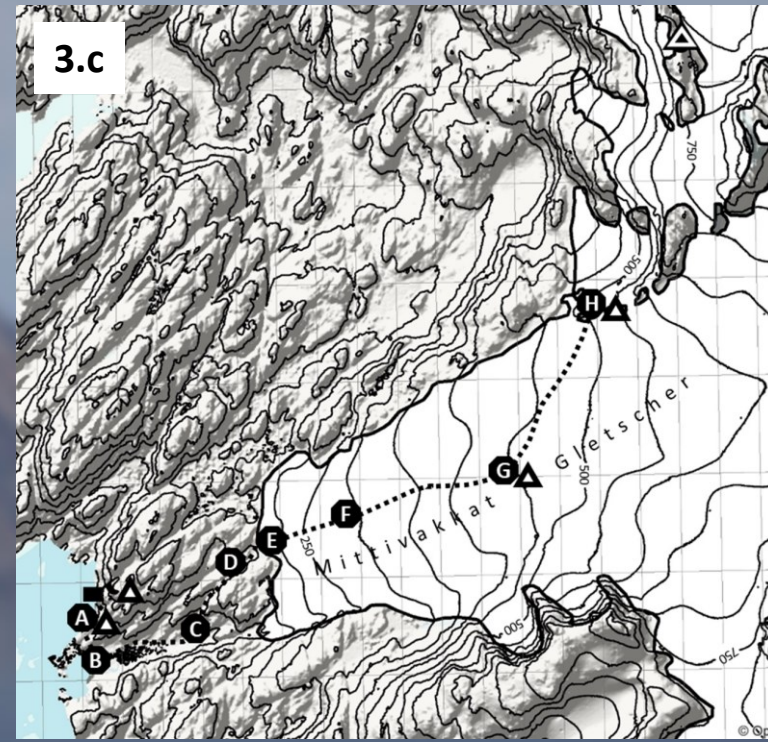
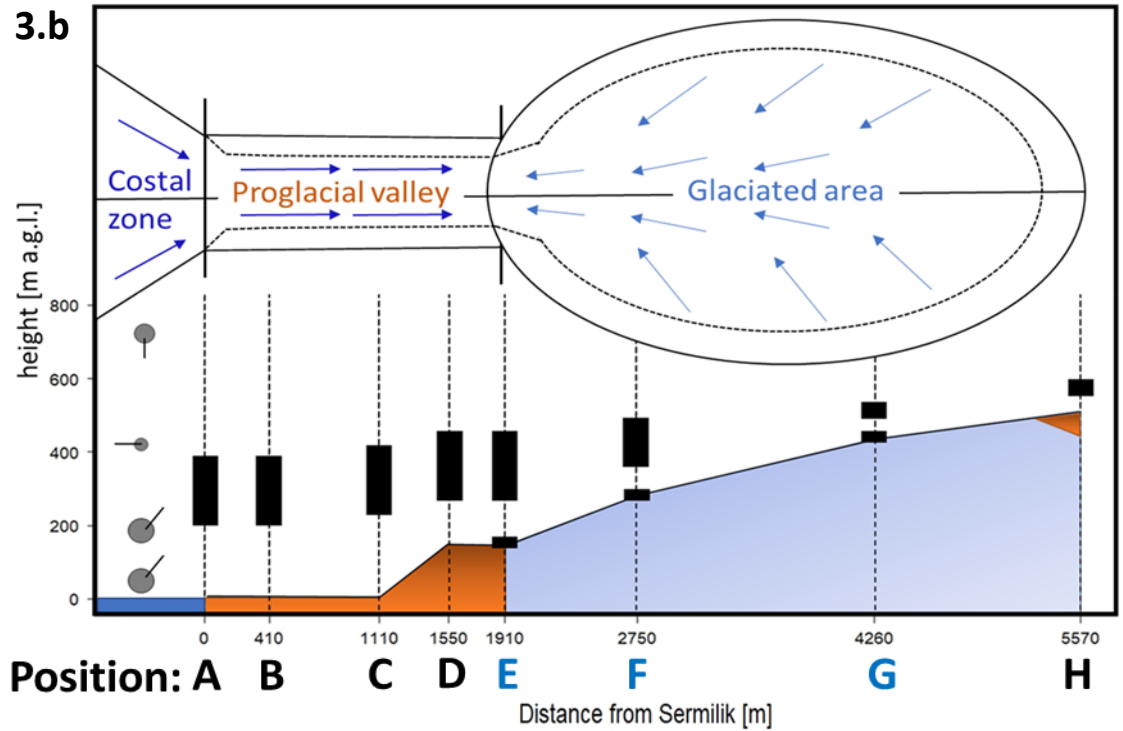
# Inversion characteristics during the field campaign



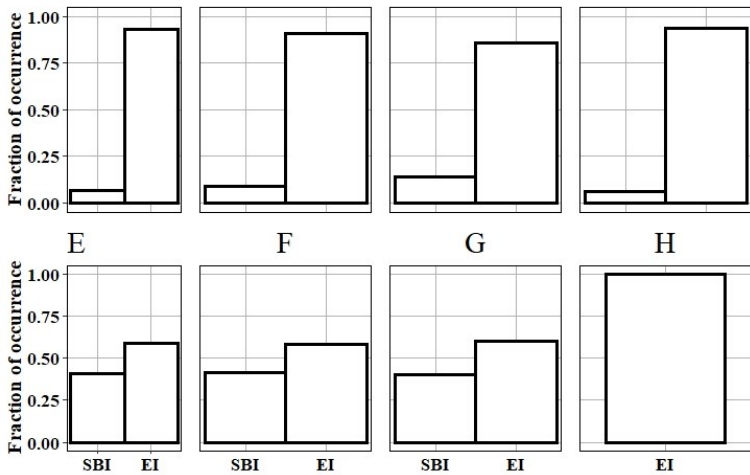
**3.a** Inversion Type frequency Drone



**3.b**



**3.d**



We found inversions in all the drone profiles; 48 SBIs and 206 EIs (fig. 3.a).

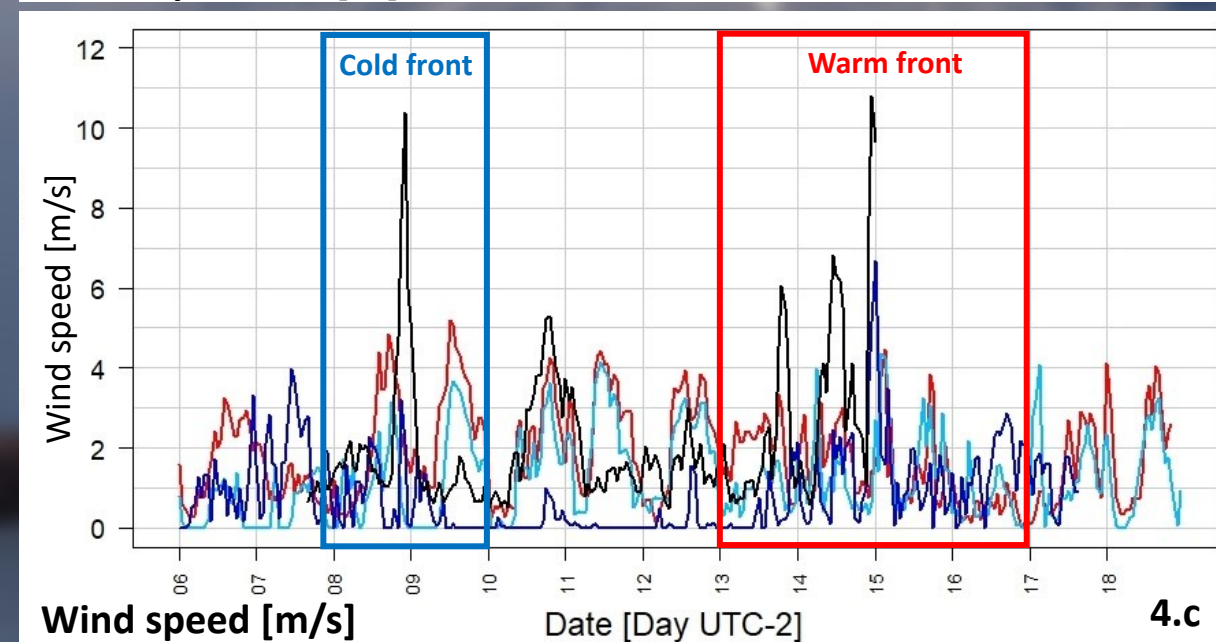
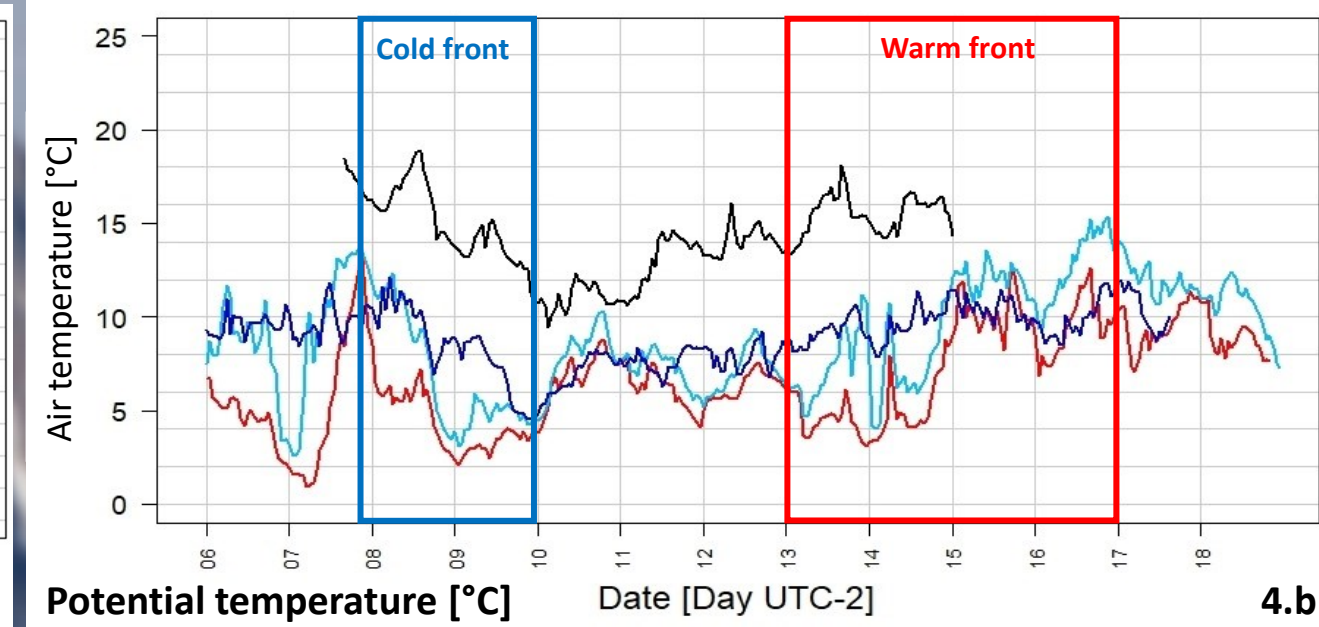
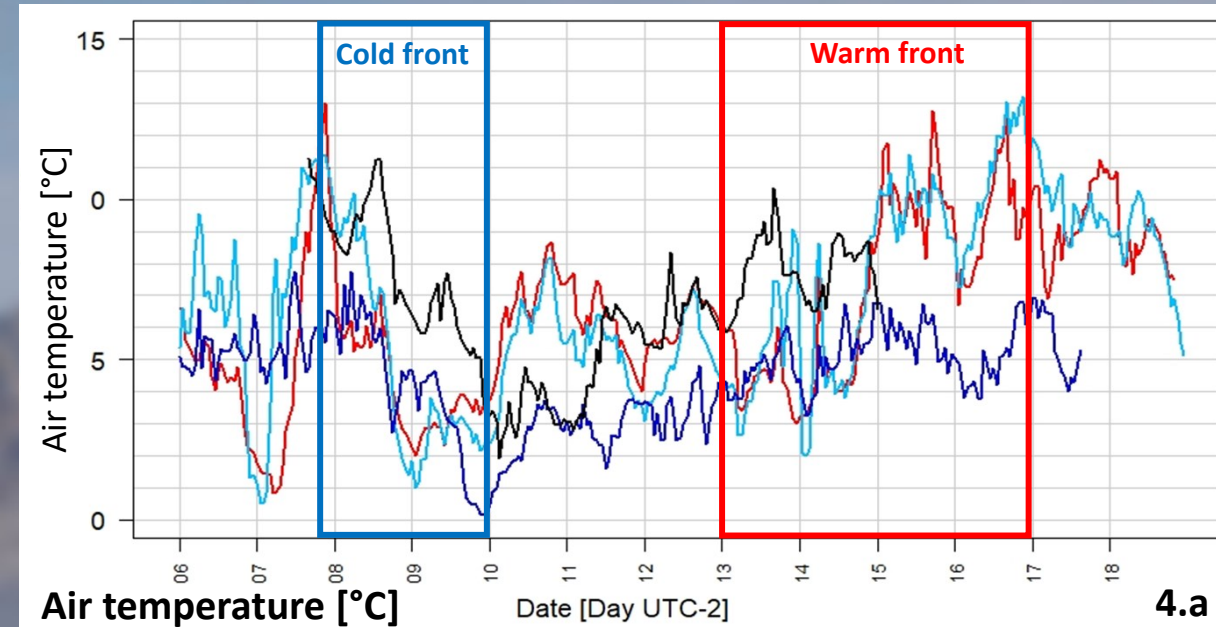
The profiles close to the sea (A, B) and above solid rock or sand (A, B, C, D, H) (fig. 3.b & 3.c) show frequent EI and seldom SBI. Frequent SBI at position E, F and G due to the glacier atmosphere and just EIs at position H (fig. 3.d).

We developed a conceptual model based on our observations during the field campaign (fig. 3.b). It shows the typical inversion characteristics above different surface types and typical wind directions and windspeed (at the ground derived from the AWS transect) in the observation area (Arctic landscape model adapted from HASHOLT & JAKOBSEN 2008).

# Inversion characteristics during the field campaign



## Weather patterns



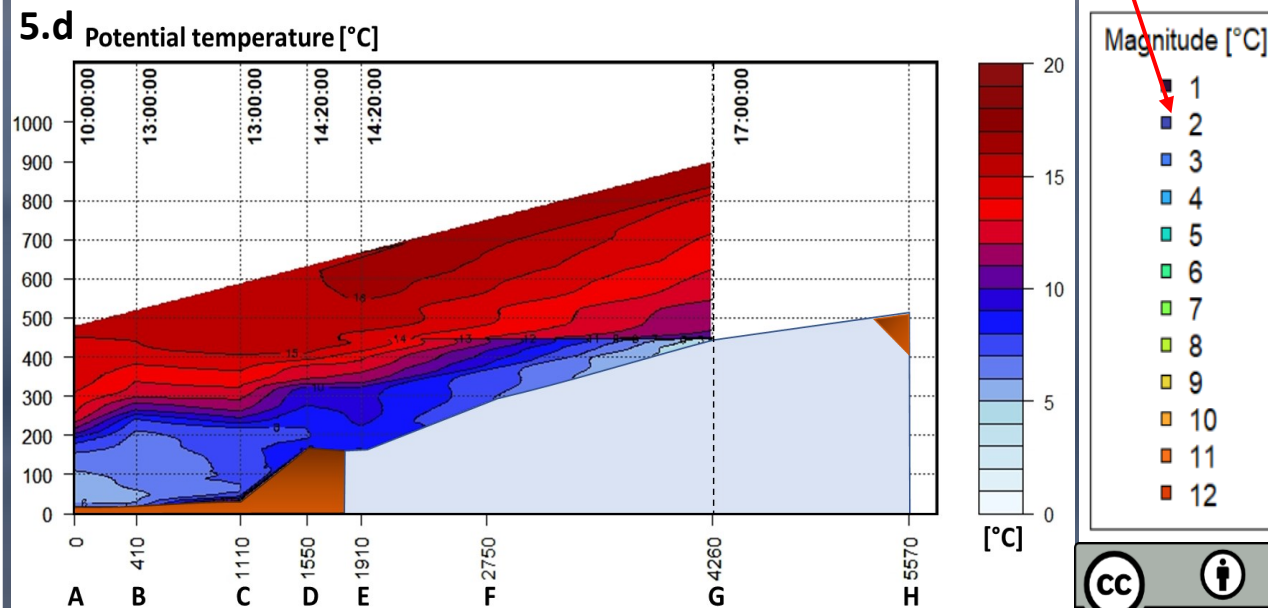
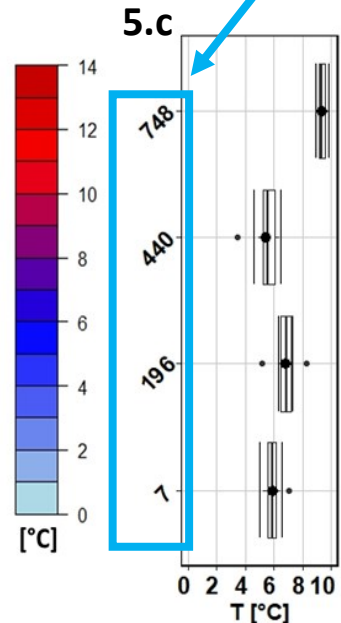
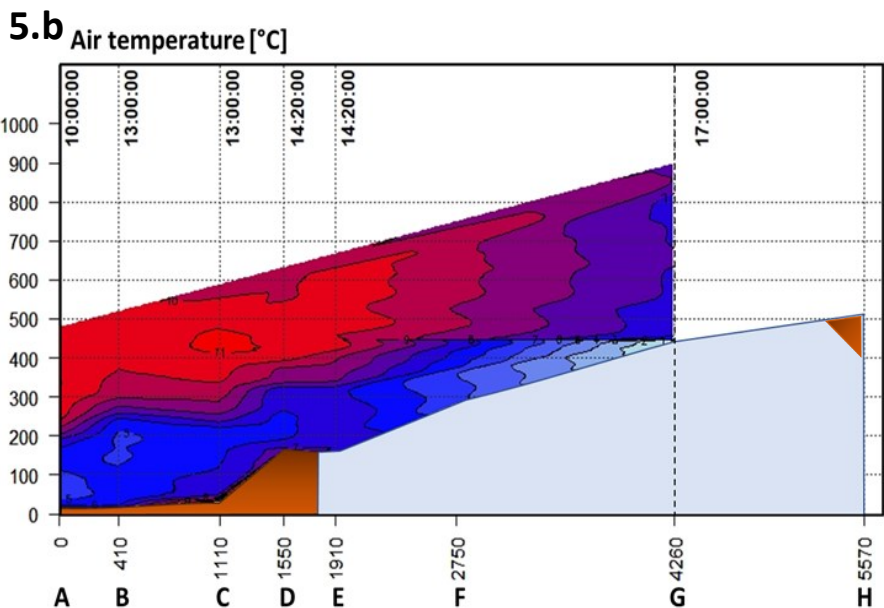
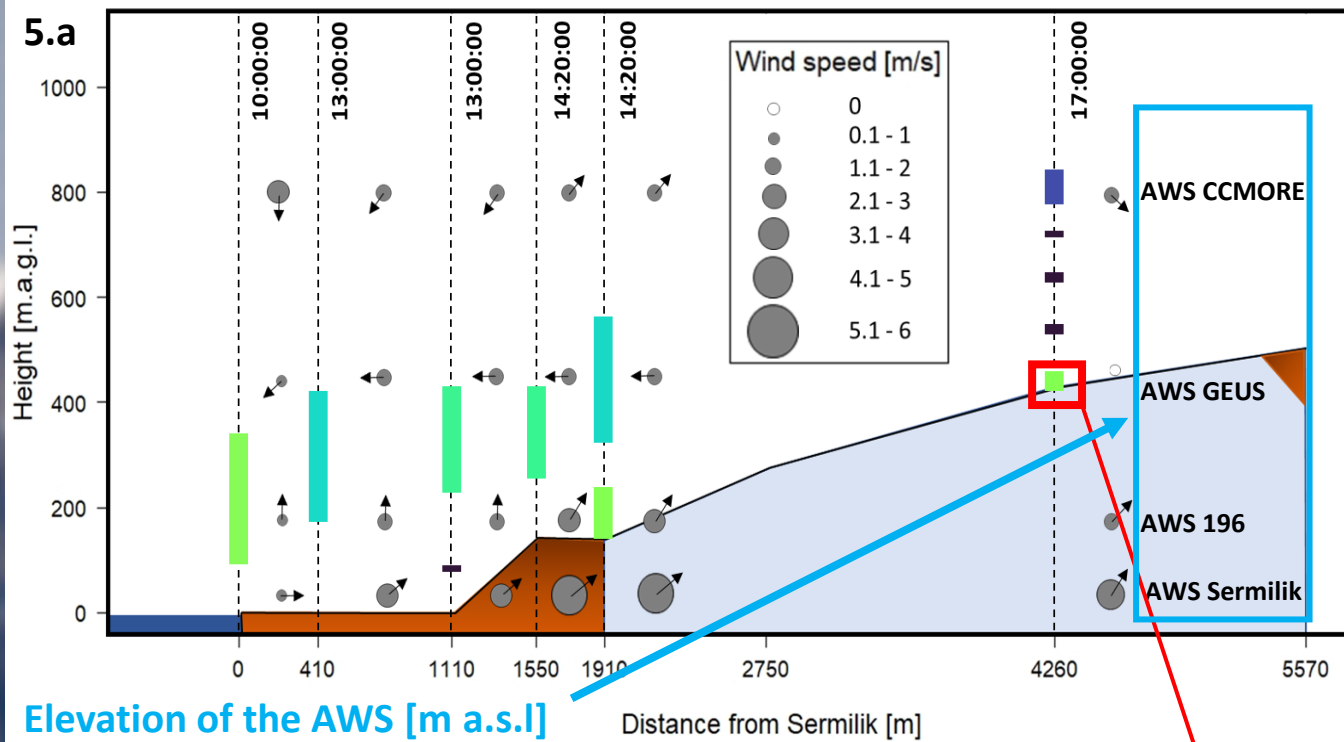
We observed two major weather shifts during the field campaign. Approximately on 8th and 9th July, a cold front passed through the observation area. Few days afterwards, between the 13<sup>th</sup> and 16<sup>th</sup> of July a warm front moved through.

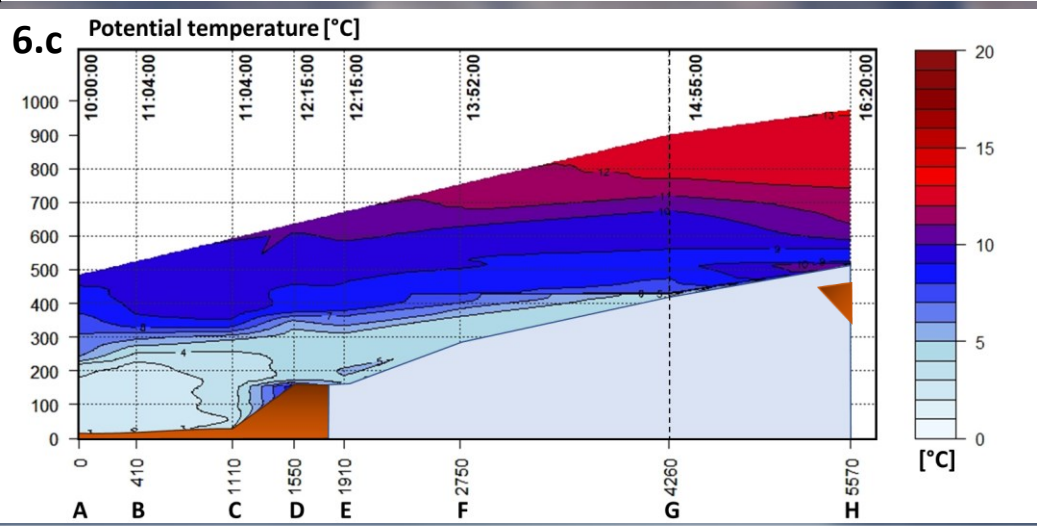
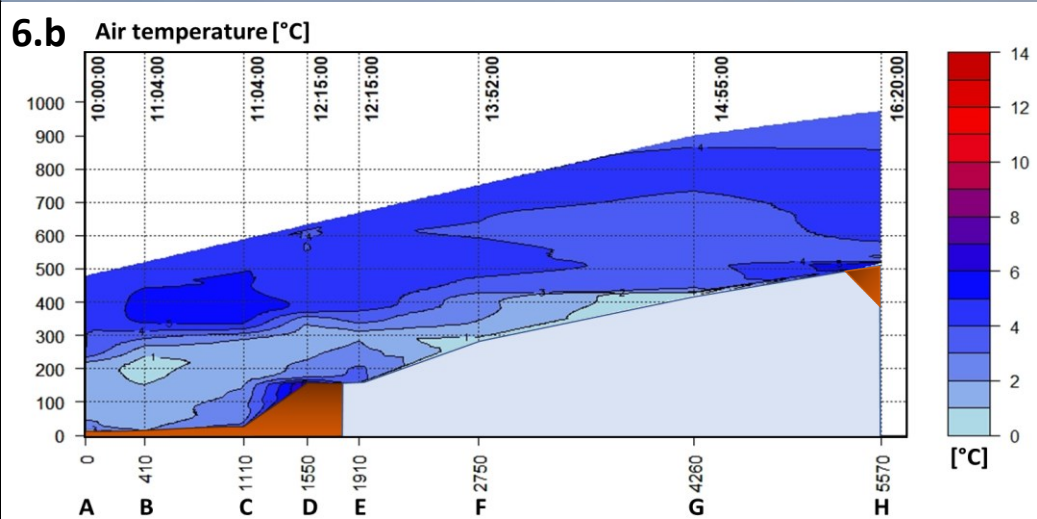
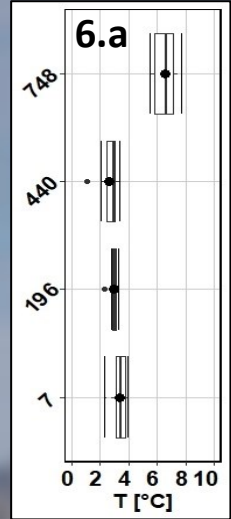
- AWS Sermilik [7 m a.s.l.]
- AWS 196 [196 m a.s.l.]
- AWS GEUS [440 m a.s.l.]
- AWS CCMORE [748 m a.s.l.]

# Inversion characteristics Cold Front Beginning: 08.07.2019

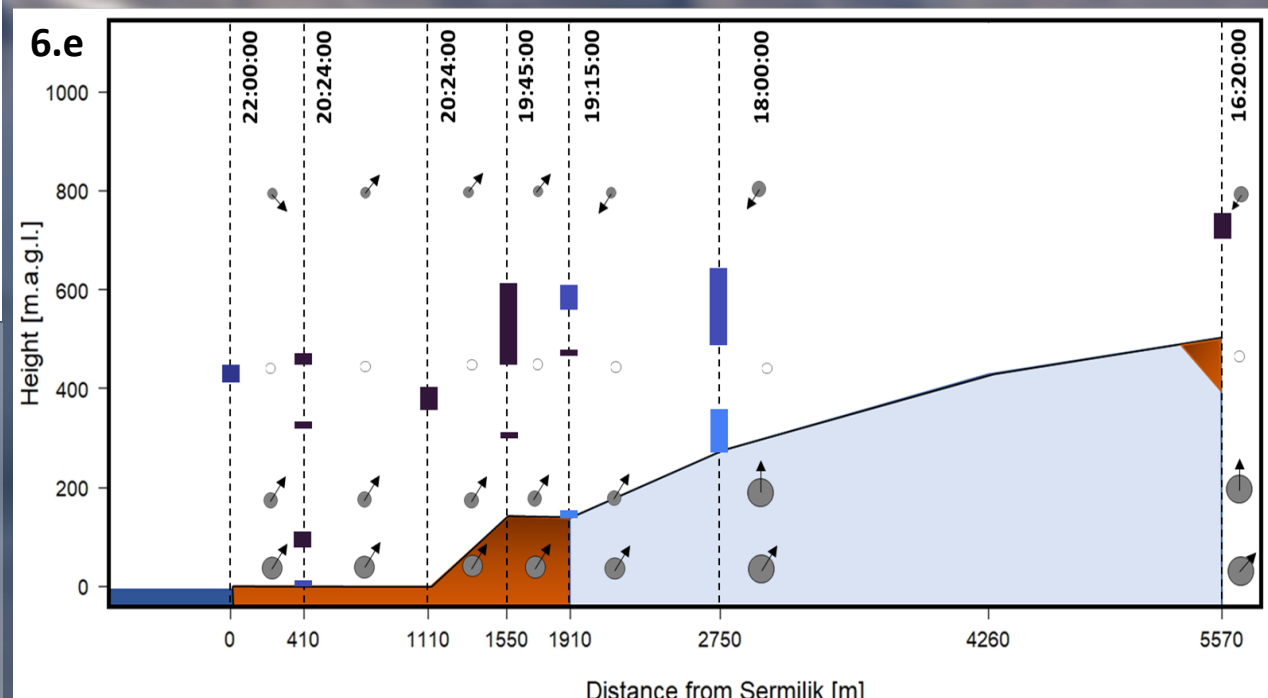
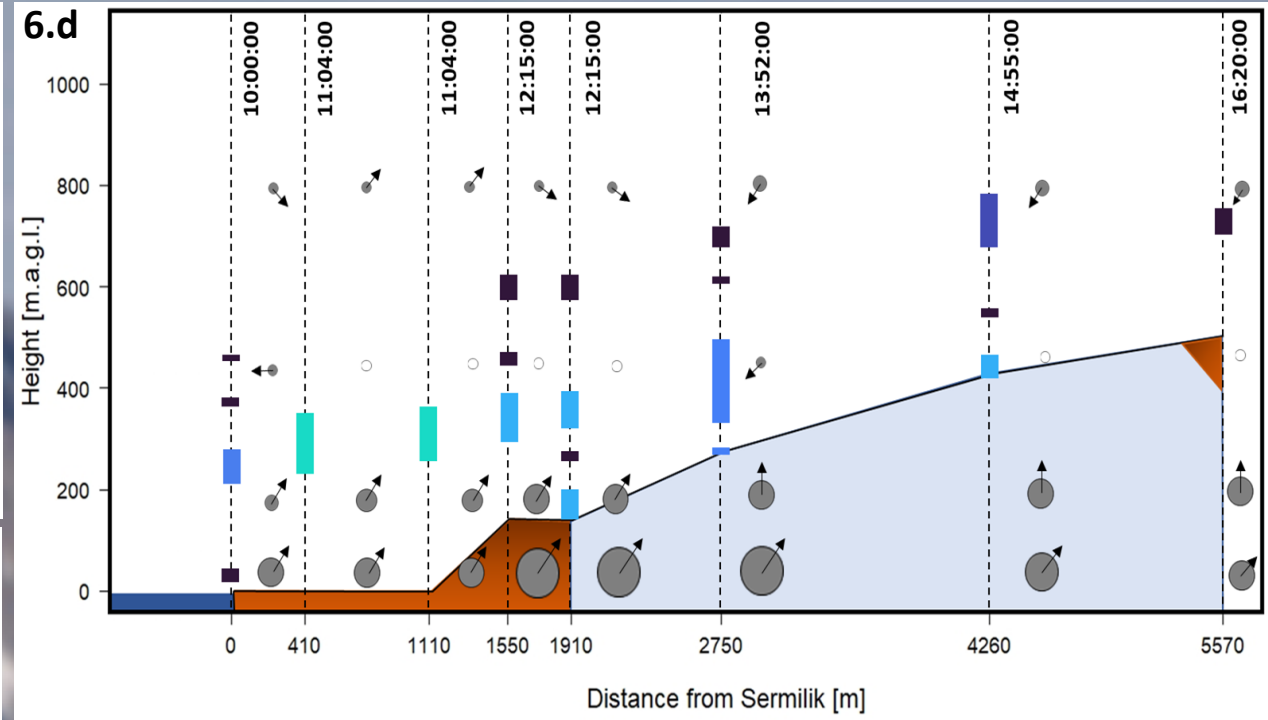
Figure 5.a shows the inversion characteristics (top, base, thickness, magnitude), wind direction (the arrow at the symbol for the wind speed) and wind speed (at the time when the profile was taken). Furthermore, we can see in the lower area the smoothed (gaussian) and linear interpolated profiles for air temperature (fig. 5.b) and potential temperature (fig. 5.c). The time in the plots indicates when the profile was taken. Figure 5.c shows the variability of the air temperature observed at the different AWS while the whole transect (fig. 5.b) was taken (between 10 to 17 o'clock UTC-2). To show that the total temperature change was smaller than the variability we measured.

During the cold front warm air is getting pushed up leading to strong EI. The sea breeze is peaking up creating a mixed unstable layer topped with a stable layer (fig. 5.b & 5.c.). As soon as the cold front is reaching the higher elevations (AWS CCMORE) wind speed is peaking up (more than 10 m/s) (fig. 4.c & 5.a) to one of the highest during the field campaign which encouraged the development of a mixed lower planetary boundary layer.





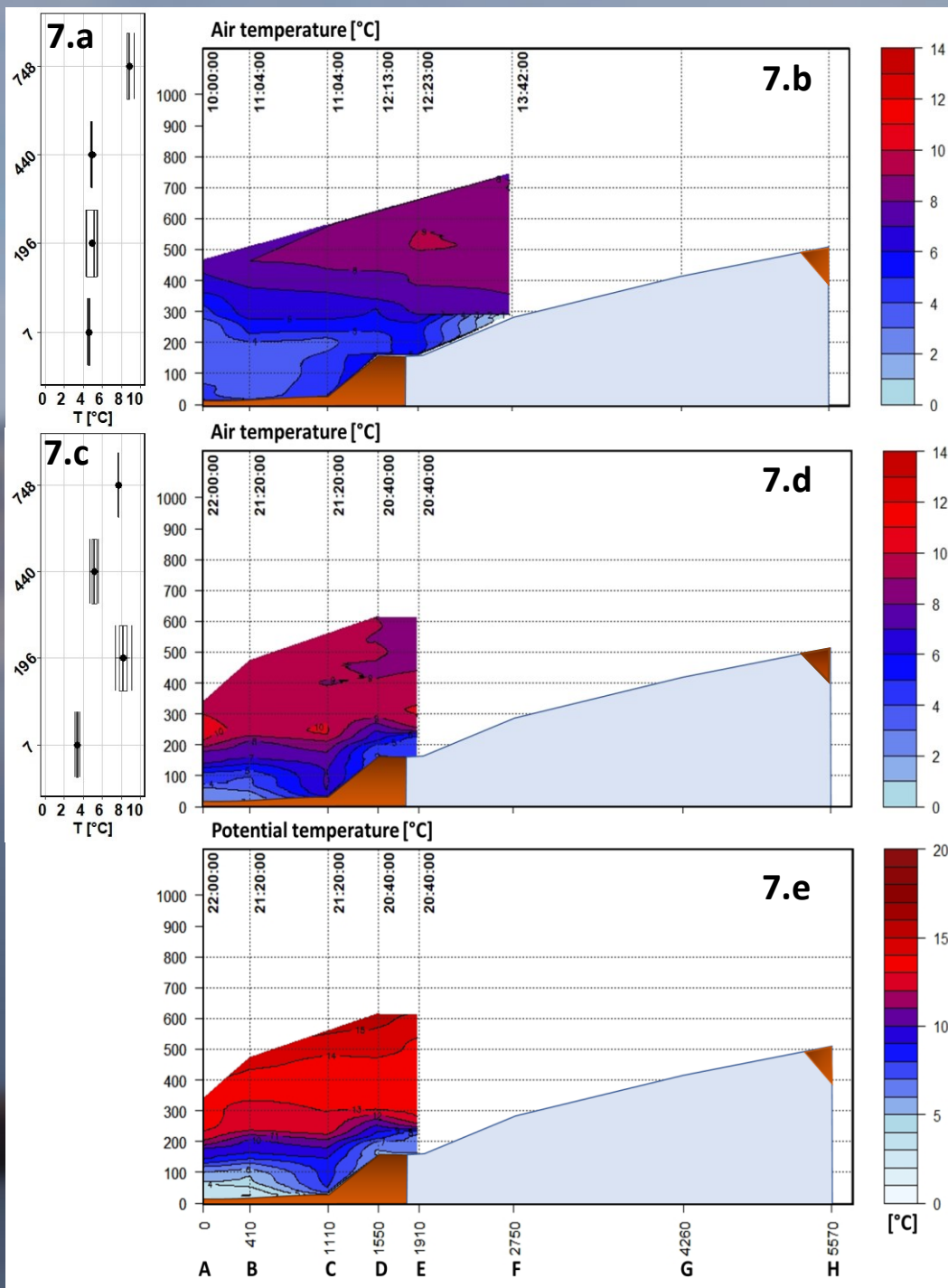
After the cold front passed the wind speed decreases at higher elevations. But we can observe a relatively strong sea breeze which is peaking up over the day (fig. 4.c, 6.d & 6.e). This strong sea breeze creates again, despite the cold air mass after the cold front, slightly stable EI inversions (fig. 6.b & 6.c with less magnitude (temperature difference inside the inversion layer). But with the weaken of the sea breeze in the late afternoon, the inversion are getting weaker or break up (fig. 6.e). Figure 6.a shows the temperature variability at the different AWS while the transect in figure 6.b was taken.



# Inversion characteristics

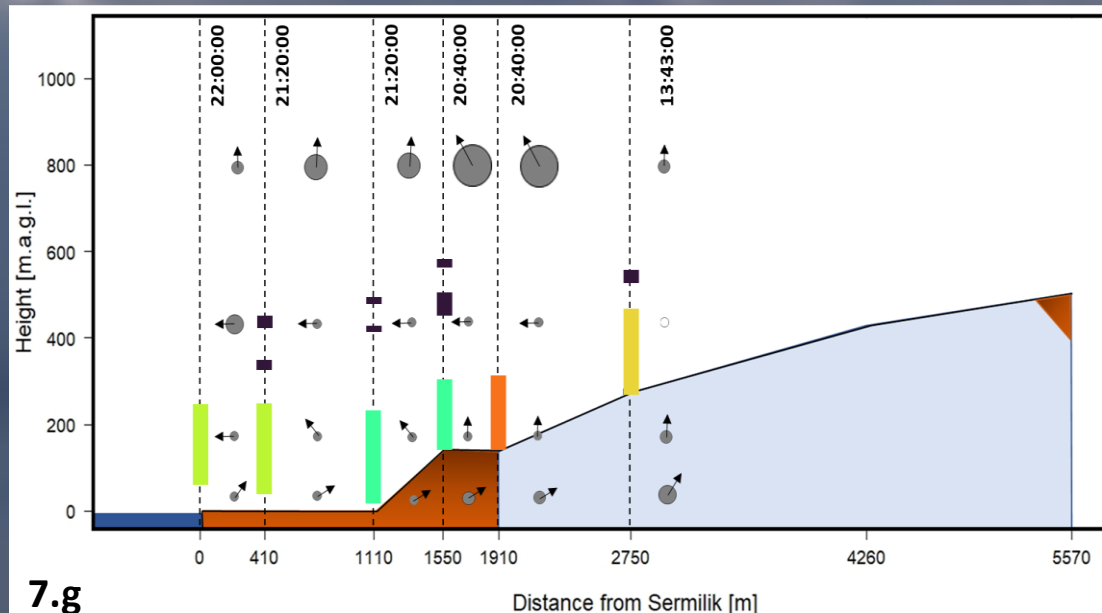
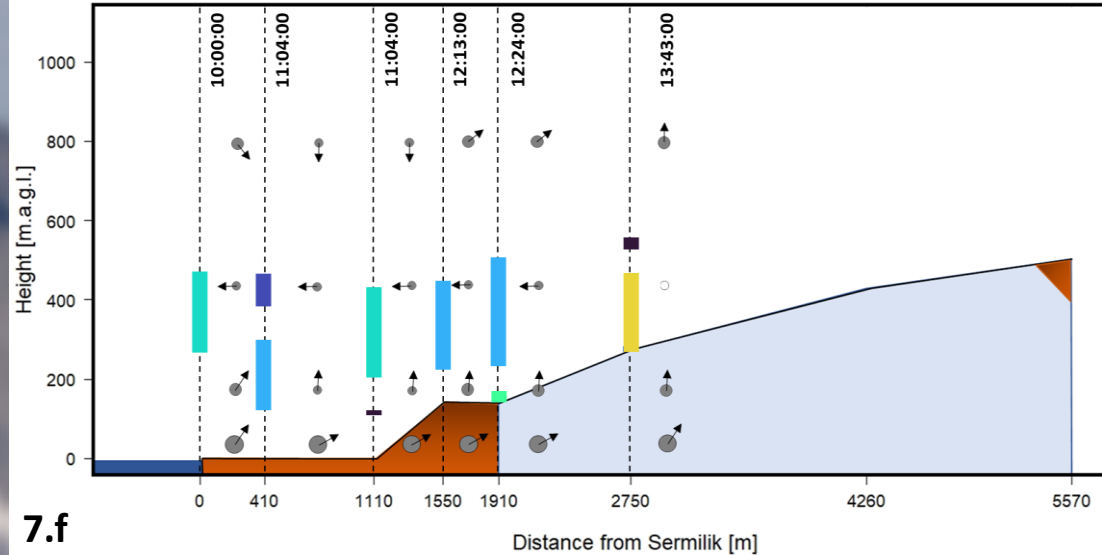
## Warm Front

### Beginning: 13.07.2019



While the warm front passes through the observation area, the air temperature is rising first in the higher elevations (fig. 7.b). We still observe a moderate sea breeze bringing cold air from the sea further inland (fig. 7.f). This situation creates a mixed unstable layer topped with a stable layer.

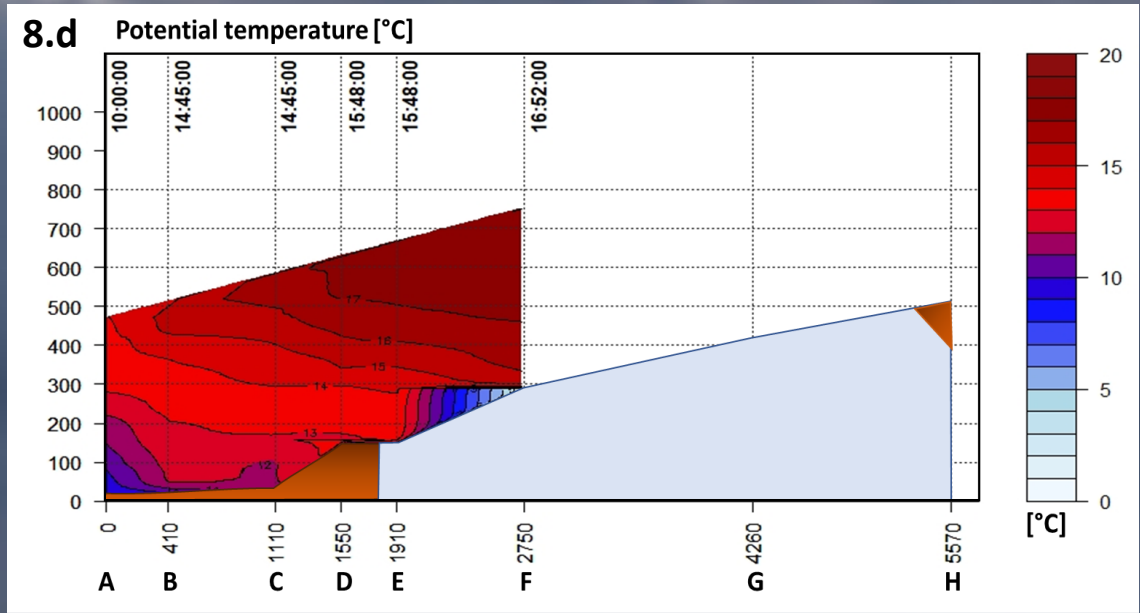
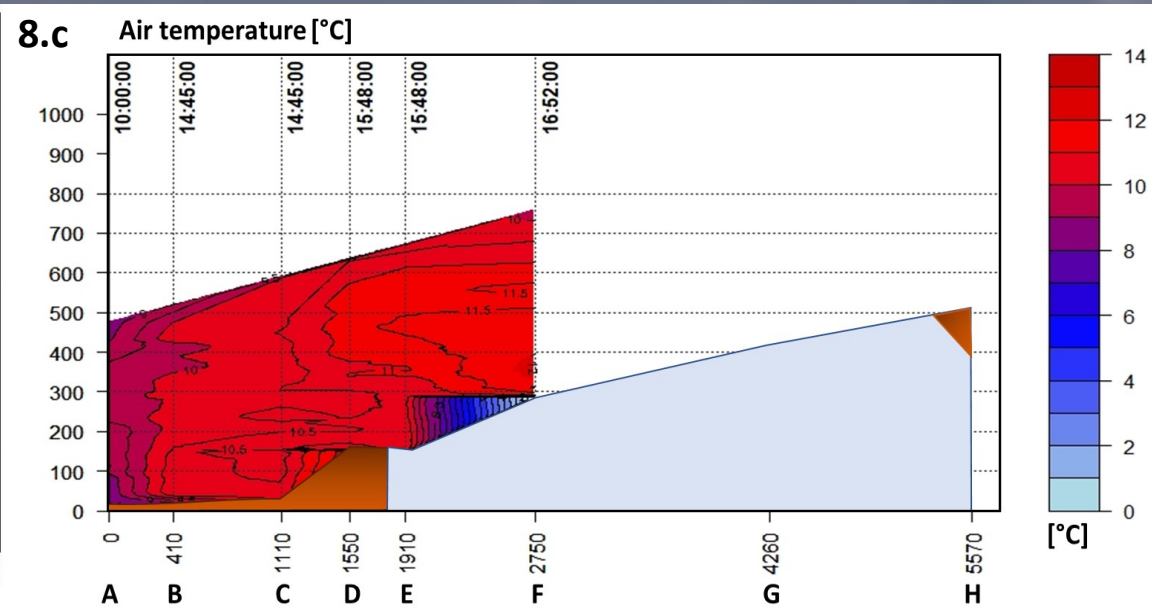
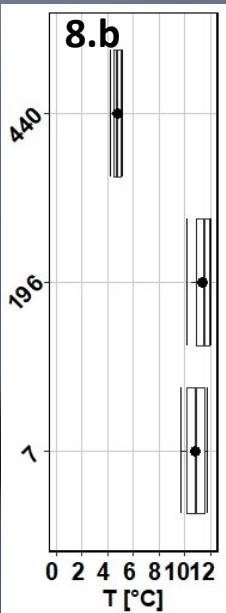
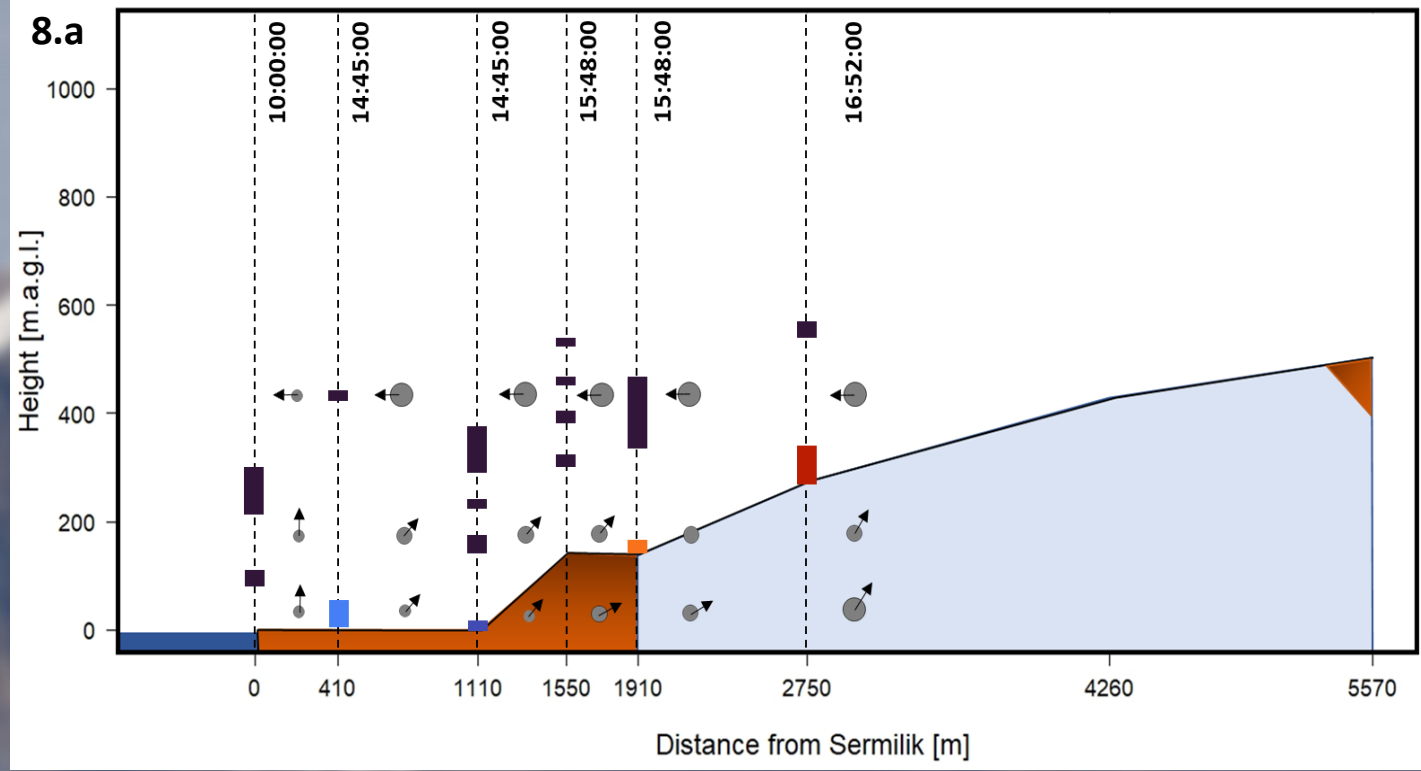
At higher elevations (AWS CCMORE), the wind is peaking up while in the lower area the wind calms down (fig. 4.c & 7.g). Furthermore, we can notice a temperature drop at higher elevations (AWS CCMORE) (fig. 4.a). This cold strong wind pushes down the stable layer and leads to thick EI with high magnitudes (fig. 7.f, 7.d & 7.e).



7.g

# Inversion characteristics Warm Front End: 16.07.2019

During the warm front period, the wind is peaking up regularly in the late afternoon at higher elevations (AWS CCMORE and GEUS) (**fig. 4.c**) reaching its peak on the 14<sup>th</sup> at around midnight with wind speed of more than 10 m/s. While the wind speed is quite high in higher elevation it is relatively weak at lower elevations (AWS Sermilik & AWS 196) (**fig. 4.c & 8.a**). It is one of the lowest wind speeds that we observed during the whole measurement period. At the 16<sup>th</sup> the warm front passed already and the cold air at the ground is eroded and replaced by warm air (**fig. 8.c**). This leads together with the weak sea breeze to thin and weak inversions (**8.a & 8.c**).





# Acknowledgment

Our sincere thanks goes to INTERACT - International Network for Terrestrial Research and Monitoring in the Arctic, which funded the whole field campaign and made this research possible.

Furthermore we would like to thank all the data providers. Data were provided by PROMICE, which is funded by the Danish Ministry of Climate, Energy and Building, operated by the Geological Survey of Denmark and Greenland and conducted in collaboration with the National Space Institute (DTU Space) and Asiaq (Greenland Survey). WMO synoptic meteorological data from the station in Tasiilaq were provided by The Danish Meteorological Institute.

# Bibliography

GILSON, G. F., JISKOOT, H., CASSANO, J. J., GULTEPE, I., & JAMES, T. D. (2018). The Thermodynamic structure of Arctic coastal fog occurring during the melt season over East Greenland. *Boundary-Layer Meteorology*, 168(3), 443-467.

HASHOLT, B., & JAKOBSEN, B. H. (2008). 75 years of research at the Sermilik Station: 1933–2008. *Geografisk Tidsskrift-Danish Journal of Geography*, 108(1), 1-4.

KAHL, J. D. (1990). Characteristics of the low-level temperature inversion along the Alaskan Arctic coast. *International journal of climatology*, 10(5), 537-548.

MERNILD, S. H., & LISTON, G. E. (2010). The influence of air temperature inversions on snowmelt and glacier mass balance simulations, Ammassalik Island, Southeast Greenland. *Journal of Applied Meteorology and Climatology*, 49(1), 47-67.

YU, L., YANG, Q., ZHOU, M., ZENG, X., LENSCHOW, D. H., WANG, X., & HAN, B. (2019). The Intraseasonal and Interannual Variability of Arctic Temperature and Specific Humidity Inversions. *Atmosphere*, 10(4), 0-14.